**Electrodeposition of Single nm Size Pt Nanoparticles at a Tunneling Ultramicroelectrode and the Determination of Fast Heterogeneous Kinetics for Ru(NH$_3$)$_6$$^{3+}$ Reduction**

Jiyeon Kim and Allen J. Bard

Supporting information

**(1) Quantitative analysis of current−time transients for the electrodeposition of a single Pt NP on TUME (equation S1, S2)**

**(2) Nucleation Exclusion Zone and a single Pt NP.(equation S3, S4)**

**(3) Intactness of TUME studied by voltammetry. (Figure S1)**

**(4) Electrochemistry vs. Tunneling at a given Pt NP. (equation S5, S6, S7, Figure S2) –S6**

**(5) Simulated voltammograms fitted with experimental curves at given Pt NP/TUME (Figure S3)**

**(1) Quantitative analysis of current−time transients for the electrodeposition of a single Pt NP on TUME**

The transient current-time curves are analyzed based on the theoretical model provided by Kucernak and coworker.[S1] The current ($i$) as a function of both time and potential for the growth of an electrodeposited particle under combined kinetic and diffusion control, and the corresponding radius ($r$) of the growing particle as a function of time are given as,

$$i(t) = \frac{ABFHn(\sqrt{A^2+8ABV_Mt}-A)^2}{2C^3\sqrt{A^2+8ABV_Mt}} \tag{S1}$$

$$A = c^*DFn$$

$$B = \frac{j_0^2}{Fn}\left(\exp\left(\frac{2\alpha nF\Delta E}{RT}\right) - \exp\left(\frac{(2\alpha-1)nF\Delta E}{RT}\right)\right)$$

$$C = j_0\exp\left(\frac{\alpha nF\Delta E}{RT}\right)$$

$$r(t) = \frac{\sqrt{A^2+8ABV_Mt}-A}{2C} \tag{S2}$$

where $c^*$ is a bulk concentration of $PtCl_6^{4-}$, $D$ is a diffusion coefficient of $PtCl_6^{4-}$ ($1.3 \times 10^{-5}$ cm$^2$/s), $F$ is the Faraday constant (96485 C/mol), $n$ is a transferred electron number ($n = 4$), $\alpha$ is transfer coefficient ($\alpha = 0.5$), $R$ is the gas constant, $T$ is a temperature (298 K), $\Delta E$ is an applied potential, $H$, a shape factor ($H = 4\pi$ for a spherical or $2\pi$ for hemispherical geometries), $V_M$, a molar volume ($V_M = 13.9$ cm$^3$/mol), $j_0$, an exchange current density ($8 \times 10^{-6}$ A/cm$^2$)[S1] and $t$, time (s).

The electrodeposition was performed in 100 μM $H_2PtCl_6$, 5 mM $H_2SO_4$ solution or 10 μM $H_2PtCl_6$, 0.5 mM $H_2SO_4$ solution under a constant potential of 0.15 V or −0.27 V vs. Ag/AgCl, respectively. Experimental current-time transients in both cases (solid lines) are shown in Figure 2, where the theoretical curves (dotted lines) simulated by equation S1 are overlapped. Parameters used in these simulations were $\alpha = 0.5$, $n = 4$, $H = 4\pi$, $T = 298$ K, $V_M = 13.9$ cm$^3$/mol, and $D = 1.3 \times 10^{-5}$ cm$^2$/s with $c^* = 1 \times 10^{-7}$ mol/cm$^3$, $\Delta E = 91.3$ mV for Figure S1a and $c^* = 1 \times 10^{-8}$ mol/cm$^3$, $\Delta E = 511$ mV for Figure 2b, respectively. In this analysis, the only freely adjustable parameter was the potential, $\Delta E$. Before forming a stable nucleus, the direct electron tunneling from Pt UME to $PtCl_6^{2-}$ in electrolyte solution across $TiO_2$ layer requires additional overpotentials to reduce $Pt^{4+}$ due to the low tunneling probability attributed to the low density of state (DOS) in a redox molecule, $PtCl_6^{2-}$ as well as its diluted concentration.[S2] Once a stable nucleus is formed and grown to NP, NP provides more DOS, thus increases the tunneling probability.[S2] Subsequently, NP mediates such a reduction reaction of $Pt^{4+}$ further and spontaneous growth can then easily proceed. In that sense, defining an accurate potential in a given TUME system is quite ambiguous, so that we consider it a freely adjustable parameter in this analysis. Here, we called the determined $\Delta E$ from the above theoretical simulation an effective potential, $E_{eff}$ exerted on TUME during nucleation and growth of Pt NP. At smaller potential, $E_{eff} = 91.3$ mV (Figure 2a), the transient current response shows kinetically controlled behavior with quadratic increase with $t$, while a mass transfer controlled behavior with $t^{1/2}$ dependence was observed at larger potential, $E_{eff} = 511$ mV (Figure 2b).[S1] The corresponding radius changing with $t$ at a determined $E_{eff}$ using equation S2 is also depicted in Figure 2c and 2d. In this simulation, 14.4 nm and 30 nm radii of Pt NPs were estimated at the end time point,

which are close to the estimation from integrated charges as well as SEM observation. Based on this consistency, we verified the determined $E_{eff}$.

**(2) Nucleation Exclusion Zone and a single Pt NP.**

We introduce a nucleation exclusion zone representing an area where the nucleation rate has dropped by one order of magnitude surrounding a growing particle as reported elsewhere.[S1] The distance from a growing particle within which the nucleation rate decreases by an amount $J_{rel}$ of the value on the electrode surface is,

$$\rho(t) = \frac{(\sqrt{A^2 + 8ABV_M t} - A)^3}{16 D c_\infty V_M C^3 t (1 - J_{rel}^{\frac{1}{1+n_k}})} \tag{S3}$$

where $A$, $B$, and $C$ have the same definition as above, $J_{rel}$ is a nucleation cutoff parameter, and $n_k$ is the minimum number of atoms for a stable nucleus, 30 to 40 atoms. Such a $\rho$ is expressed as a function of time during the growth of a particle under a diffusion or kinetic control depending on the applied potential. Subsequently, the dimensionless form of the above distance can be derived by dividing eq S3 by eq S2,

$$\frac{\rho(t)}{r(t)} = \frac{(\sqrt{A^2 + 8ABV_M t} - A)^2}{8 D c_\infty V_M C^2 t (1 - J_{rel}^{\frac{1}{1+n_k}})} \tag{S4}$$

In reality, the nucleation exclusion zone can be defined as the distance where the nucleation rate is reduced to by factor of 10, i.e. $J_{rel} = 0.1$, with $n_k = 35$. Using eq S4 with given $J_{rel}$ and $n_k$, we could plot a dimensionless size of nucleation exclusion zone ($\rho$) respect to the actual size of the particle as a function of time at given $E_{eff}$ determined as above and precursor concentrations

(Figure 5a). When the particle is growing under diffusion control at a large potential, $E_{eff} = 0.51$ V with 10 μM $PtCl_6^{2-}$ (Figure 2b), the nucleation probability is almost instantaneously reduced by at least one order of magnitude within c.a. 16 times radius of the growing particle (blue curve in Figure 5a). It means that it is unlikely to have another nucleation within 80 nm distance around a 5 nm radius particle. Such a nucleation exclusion zone helps the production of a single nucleus, since there will be a significant reduction in the concentration of precursor in the area surrounding a growing particle, thus reducing the probability of nucleating another new particle. In that sense, a small electrode, a large potential and low precursor concentration are important criteria for forming a single particle. In contrast, when the growth of particle is under kinetic control at $E_{eff} = 0.091$ V and 100 μM $PtCl_6^{2-}$ (Figure 2a), the nucleation exclusion zone only reaches within a few radii of a growing particle even after appreciable time (black solid curve in Figure 5a). Now, it may be possible to form multiple smaller nuclei at other points in a given area on the TUME.

**(3) Intactness of TUME studied by voltammetry.**

To make sure that all faradaic currents are attributed to presence of Pt NP not the leakage on a TUME, we compared voltammograms before and after electrodeposition of Pt NP. For this test, we cleaned Pt NP/TUME in DI water by vigorously shaking, thus dropping a Pt NP from TUME and ran voltammetry in in 5 mM $Ru(NH_3)_6^{3+}$ , 0.1 M $KNO_3$. In Figure S1, both voltammograms from bare TUME before electrochemistry and after electrochemistry followed by vigorous cleaning in water are well overlapped showing no discernible faradaic current to confirm the intactness of $TiO_2$ layer.
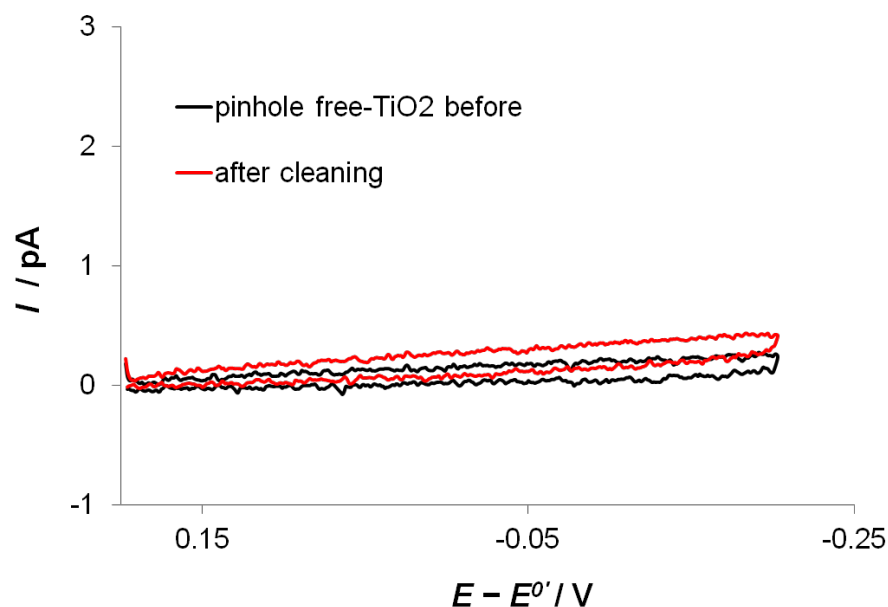
Figure S1. Cyclic voltammograms in 5 mM $Ru(NH_3)_6^{3+}$, 0.1 M $KNO_3$ with bare TUME before electrodeposition of Pt NP (black solid curve) and after all electrochemistry with electrodeposited Pt NP followed by cleaning in water (red solid curve).

**(4) Electrochemistry vs. Tunneling at a given Pt NP.**

In the K-L treatment, we considered the overall electrochemical reaction at a Pt NP/TUME governed by the rates of consecutive three processes of (a) a direct tunneling from Pt UME to Pt NP through $TiO_2$ layer (b) a mass transfer of redox species from bulk solution to near a Pt NP surface and (c) an ET to redox species at Pt NP. Therefore, the overall current density at Pt NP/TUME has contributions from tunneling, mass transfer and ET, and expressed as,[S3]

$$\frac{1}{j} = \frac{1}{j_{tun}} + \frac{1}{j_{et}} + \frac{1}{j_{mt}} \tag{S5}$$

To predict whether a Pt NP/TUME is under tunneling or electrochemical control, we compare the ratio of the tunneling and electrochemical current densities when the electrochemistry is limited by mass transfer. Thus, $j_{tun}/j_{mt}$ is given as reported previously,[S3]

S6

$$\frac{j_{tun}}{j_{mt}} = -\frac{q^2\eta}{8\pi \ln 2 FDC^* r_0 h}\left[\frac{w_0+r_0}{w_0}\left(\frac{2a\varphi^{1/2}w_0+0.486}{2a\varphi^{1/2}w_0+1.451}\right)-1\right]e^{-2a\varphi^{1/2}w_0} \qquad (S6)$$

where $q$ is the elementary charge, $h$ is the Planck constant, $a = \left(\frac{2m}{\hbar^2}\right)^{1/2} \approx 0.512 \text{ eV}^{-1/2} \text{ Å}^{-1}$, $\varphi$, the offset between the Fermi level of the metal and the barrier potential ($\varphi$ = 1.3 eV for TiO$_2$ layer), $w_0$, the thickness of the TiO$_2$ layer, $r_0$, a Pt NP radius, $\eta$, a potential difference between the UME and Pt NP , $C^*$, a bulk concentration (5 mM), $D$, a diffusion coefficient of Ru(NH$_3$)$_6$ $^{3+}$ (7.4×10$^{-6}$ cm$^2$/s) and the other terms are as defined above. In Figure S2a, we plot the current density ratio as a function of $w_0$ and $r_0$ at a given condition. Especially, at c.a. 1 nm thick TiO$_2$ layer, $j_{tun}$ / $j_{mt}$ above c.a. 0.7 nm radius of Pt NP is positioned near the mass transfer controlled regime due to the large $j_{tun}$. Since the smallest term in eq S5 will be dominant, the overall current density at Pt NP is controlled appreciably only by mass transfer and ET, and expressed as,

$$\frac{1}{j} = \frac{1}{j_{et}} + \frac{1}{j_{mt}} \qquad (S7)$$

However, as the $r_0$ gets smaller than 0.7 nm, $j_{tun}$ / $j_{mt}$ drastically decreases with decrease in $r_0$, thereby the tunneling more appreciably influences on the overall current response at smaller Pt NP. We illustrated this situation in Figure S2b, which is a cross-sectional plot of Figure S2a at $w_0$ = 10.5 Å.
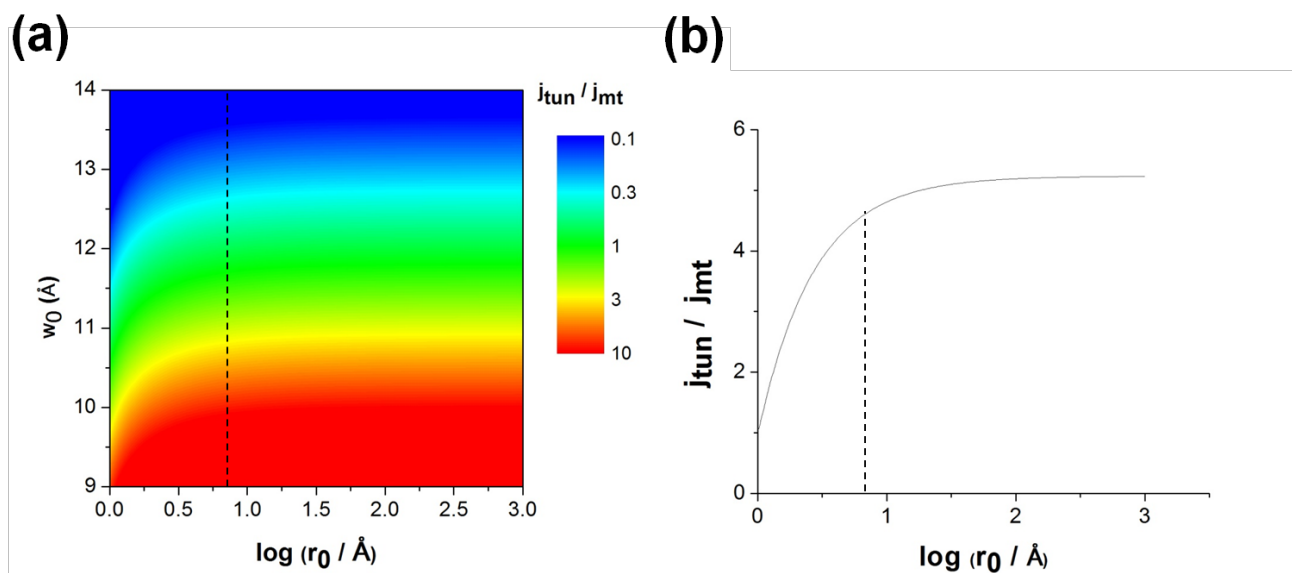
Figure S2. (a) Ratio of tunneling and electrochemical current densities as a function of $w_0$ and $r_0$ for $\varphi = 1.3$ eV, $\eta = -200$ mV, $D = 7.4 \times 10^{-6}$ cm$^2$ s$^{-1}$, and $C^* = 5$ mM. (b) Cross-sectional plot of Figure S2a, $j_{tun} / j_{mt}$ as a function of radius of a Pt NP, $r_0$ at the thickness of TiO$_2$ layer, $w_0 = 10.5$ Å. Each dotted line denotes 0.7 nm radius of Pt NP.

## (5) Simulated voltammograms fitted with experimental curves at given Pt NP/TUME

We theoretically confirmed the measured kinetic parameters with finite element analysis using COMSOL MULTIPHYSICS (v. 4.2a). The theoretical voltammograms simulated for $k^0 = 36$ cm/s, $\alpha = 0.5$ showed a good agreement with all spans of experimental curves from the smallest, 0.7 nm to the largest radius, 41.6 nm of Pt NP/TUME. A clear transition from Nernstian behavior to kinetic control can be seen in the voltammograms normalized respect to each limiting current.
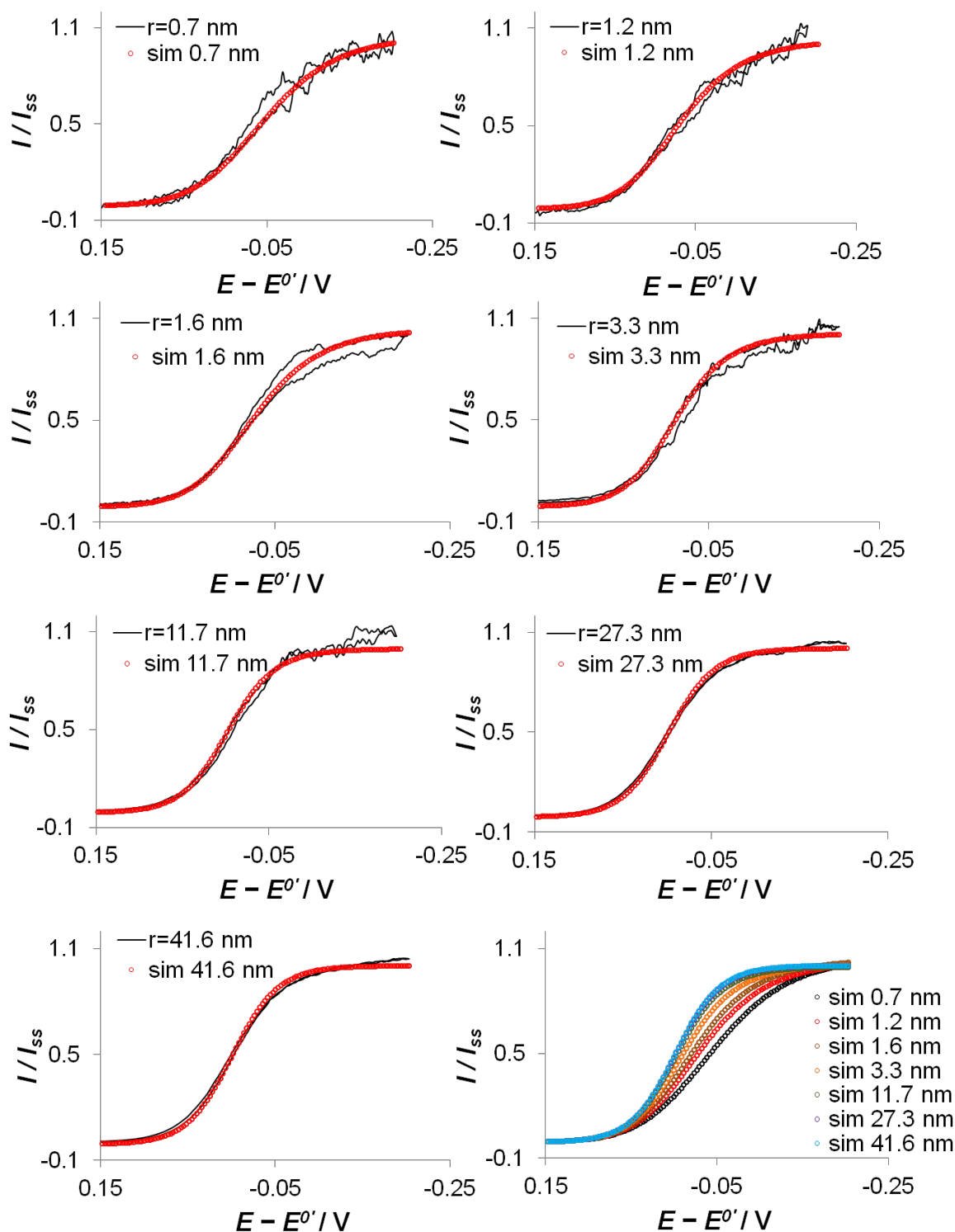
Figure S3. Theoretically simulated voltammograms (open circles) for $k^0 = 36$ cm/s, $\alpha = 0.5$ fitted with experimental voltammograms (solid lines) from radii of 0.7 and 41.6 nm Pt NP/TUMEs. To show the clear difference in curve shape, voltammograms were normalized respect to each limiting current.

(S1) Chen, S.; Kucernak, A., *J. Phys. Chem. B.* **2003**, 107, 8392-8402.

(S2) Chazalviel, J.; Allongue, P., *J. Am. Chem. Soc.*, **2010**, *133*, 762-764

(S3) Hill, C.M.; Kim, J.; Bard, A.J., *J. Am. Chem. Soc*. **2015**, 137, 11321-11326.